Geosci. Model Dev. Discuss., 8, 10305–10337, 2015
www.geosci-model-dev-discuss.net/8/10305/2015/
doi:10.5194/gmdd-8-10305-2015

Geoscientific Model Development Discussions
Open Access
EGU

Improving the WRF model's simulation over sea ice surface through coupling with a complex thermodynamic sea ice model

Y. Yao, J. Huang, Y. Luo, and Z. Zhao

Ministry of Education Key Laboratory for Earth System Modeling, Center for Earth System Science, Tsinghua University, Beijing, China

Received: 8 September 2015 – Accepted: 24 November 2015 – Published: 3 December 2015

Correspondence to: J. Huang (jbh@tsinghua.edu.cn)

Published by Copernicus Publications on behalf of the European Geosciences Union.

Abstract

Sea ice plays an important role in the air–ice–ocean interaction, but it is often represented simply in many regional atmospheric models. The Noah sea ice model, which has been widely used in the Weather Research and Forecasting (WRF) model, exhibits cold bias in simulating the Arctic sea ice temperature when validated against the Surface Heat Budget of the Arctic Ocean (SHEBA) in situ observations. According to sensitivity tests, this bias is attributed not only to the simulation of snow depth and turbulent fluxes but also to the heat conduction within snow and ice. Compared with the Noah sea ice model, the high-resolution thermodynamic snow and ice model (HIGHTSI) has smaller bias in simulating the sea ice temperature. HIGHTSI is further coupled with the WRF model to evaluate the possible added value from better resolving the heat transport and solar penetration in sea ice from a complex thermodynamic sea ice model. The cold bias in simulating the surface temperature over sea ice in winter by the original Polar WRF is reduced when HIGHTSI rather than Noah is coupled with the WRF model, and this also leads to a better representation of surface upward longwave radiation and 2 m air temperature. A discussion on the impact of specifying sea ice thickness in the WRF model is presented. Consistent with previous research, prescribing the sea ice thickness with observational information would result in the best simulation among the available methods. If no observational information is available, using an empirical method based on the relationship between sea ice concentration and sea ice thickness could mimic the large-scale spatial feature of sea ice thickness. The potential application of a thermodynamic sea ice model in predicting the change in sea ice thickness in a RCM is limited by the lack of sea ice dynamic processes in the model and the coarse assumption on the initial value of sea ice thickness.

GMDD
8, 10305–10337, 2015

1 Introduction

Regional climate models (RCMs) are useful tools for understanding the processes in the polar climate system, and they have been widely used to provide detailed projections of future climate change over polar regions. As part of the Coordinated Regional Downscaling Experiment (CORDEX), the Polar-CORDEX will provide ensembles of climate simulations over the Arctic and Antarctic domains from different modeling groups around the world (Koenigk et al., 2015). The results from Polar-CORDEX are supposed to be analyzed by researchers from various disciplines, and further studies such as climate impact and adaptation in the polar region would be conducted based on these simulation results. Increasingly more modeling groups have participated in Polar-CORDEX, and the development of RCMs suitable for polar climate simulations have aroused interests within the modeling community.

Although climate models have become more sophisticated, climate simulation over the polar region remains a formidable challenge (Notz, 2012; Bourassa et al., 2013). The surface radiance budget, which exhibits marked seasonal differences between summer and winter and plays an important role in the polar climate system, has been erroneously represented in climate models for a long time (Sorteberg et al., 2007; Tjernström et al., 2008; Barton et al., 2014). From a perspective from the top of the atmosphere to the surface, researchers have attributed the bias of the surface radiation budget to the poor ability of models to properly represent both the cloud radiation effect and the stable boundary layer (Wyser et al., 2007; Vihma and Pirazzini, 2005). The Arctic cloud, particularly the mixed-phase low cloud, is misrepresented in current state-of-the-art climate models (Pithan et al., 2013; English et al., 2015). Simulating the stable boundary layer is limited not only by the relatively coarse resolution (Steeneveld et al., 2006) but also by the lack of realistic representations of small-scale physical processes, such as turbulent mixing and snow-surface coupling (Sterk et al., 2013). Moreover, considerable effort has been devoted to evaluating and improving the mi-

GMDD
8, 10305–10337, 2015

crophysics and boundary layer parameterizations (e.g., Wang and Liu, 2014; Andreas et al., 2010).

Sea ice, which distinguishes the polar climate system from other parts of the earth system, often lacks detailed treatment in current RCMs. When the ocean is covered by sea ice, the exchange of heat between air and sea and the penetration of solar radiation differ significantly from those over open water. Acting as a medium between air and sea, sea ice plays an important role in the surface energy balance over the polar region (Jin et al., 1994). Thus, a realistic simulation of the polar climate requires sea ice to be appropriately considered in the RCMs. Coupled RCMs, including interactive ocean and sea ice models, have shown benefits from a better representation of the air–ice–ocean interaction (Dorn et al., 2009). However, the relatively large resources that are required to construct the coupled modeling system and the insufficient simulation of feedbacks between the model components have limited the use of coupled RCMs (Dorn et al., 2012). To meet the urgent needs of researches and applications from different fields, atmospheric-only RCMs are still widely used in simulations of the polar climate. In these models, sea surface temperature, sea ice concentration and sea ice thickness have to be specified. Sensitivity experiments based on regional atmospheric models have shown that properly specifying the sea ice thickness and snow on ice have a considerable impact on the simulation of surface temperature (Rinke et al., 2006; Hines et al., 2015). Moreover, physical properties such as sea ice temperature are considered by thermodynamic sea ice models to provide lower boundary conditions for the atmospheric model. Thus, a failure in the energy conservation in the sea ice model can lead to bias of the surface energy balance in long-term climate simulations (Bitz and Lipscomb, 1999). However, evaluations of the performance of the thermodynamic sea ice model within RCMs are limited.

Among the atmospheric-only RCMs, the Weather Research and Forecasting (WRF) model, along with its polar-optimized version (Polar WRF), has been widely used in polar climate simulations. Previous evaluations have shown that the WRF model can reasonably simulate climatological features of the Arctic atmosphere (Cassano et al.,

GMDD
8, 10305–10337, 2015

2011). Additionally, physical credibility has been found in simulating extreme precipitation over CORDEX Arctic from a long-term climate simulation based on the WRF model (Glisan and Gutowski, 2014a, b). Moreover, the modifications included in the Polar WRF model have been validated against various observations in Greenland (Hines and Bromwich, 2008), the Arctic Ocean (Bromwich et al., 2009), Arctic land (Hines et al., 2011), and the Antarctic (Bromwich et al., 2013).

Because the WRF model was originally developed for simulations in mid-latitudes, processes associated with sea ice are described by a simplified thermodynamic sea ice model incorporated in the Noah surface scheme within the WRF model. Currently, there are few evaluations on the performance of a simplified sea ice model when it is used as part of a RCM during long-term climate simulations. How well does Noah sea ice within the WRF model represent the long-term evolution of sea ice status? If bias exists in the sea ice simulation by Noah, its contribution to the bias previously found in the surface radiation budget needs to be accounted for. To improve the simulation over the polar region by the WRF model, it is worth testing the possible added value from coupling a complex thermodynamic sea ice model. Can the simulation over the sea ice surface benefit from a more realistic simulation of sea ice thermodynamics? As mentioned above, additional information on sea ice thickness needs to be specified when the atmospheric-only RCM is used in polar climate simulations. While a complex thermodynamic sea ice model can predict the change in sea ice thickness, the RCM might be able to predict the actual sea ice thickness. How is the sea ice thickness prescribed if a complex sea ice model is coupled to the RCM? This study is conducted based on the above questions.

In this study, the Noah sea ice model is compared with a high-resolution thermodynamic snow and ice model (HIGHTSI). The offline simulations of the sea ice temperature evolution using these two sea ice models are evaluated in Sect. 3. The HIGHTSI is then coupled to the WRF model, and the coupled simulations based on Noah and the HIGHTSI sea ice model are compared in Sect. 4. The evaluation is primarily focused on the simulation over the sea ice surface to determine whether coupling

GMDD
8, 10305–10337, 2015

a complex thermodynamic sea ice model would be beneficial for regional climate simulations. In Sect. 5, we present a discussion on how to prescribe the sea thickness in an atmospheric-only regional climate simulation.

2 Models and data

2.1 WRF

The WRF model is a state-of-the-art mesoscale numerical model designed for both research and operations. It is primarily maintained by the National Centers for Atmospheric Research (NCAR) and developed by collaborative efforts from the community. The WRF model has been widely used in climate simulations, and its applications in the polar region have also provided useful information (Liu et al., 2014). Polar WRF is a polar-optimized version released after the standard WRF model. Modifications such as fractional sea ice and optimized surface energy balance over land ice and sea ice enabled the model to better simulate the polar climate (Hines and Bromwich, 2008). Moreover, some of these changes have already been added to recent versions of standard WRF releases.

In both WRF and Polar WRF, a simplified thermodynamic sea ice model that is included in the Noah land surface model is used to determine the sea ice-related properties, such as sea ice temperature and turbulent fluxes. The Noah sea ice module incorporated in WRF contains 4-layer ice together with a single-layer snow pack model. The ice growing and ablation processes are not included in Noah, and thus, the sea ice thickness must be specified. The default value for sea ice thickness is 3 m everywhere in the WRF model, and this value can be prescribed from other sources in the same way as sea ice concentration such that the spatial and temporal variations of sea ice thickness can be taken into account (Hines et al., 2015). The sea ice surface is assumed to always be covered by snow in Noah, and a lower bound (default is 0.01 m) for snow depth has to be prescribed. Under this assumption, the surface energy balance

GMDD
8, 10305–10337, 2015

would always be evaluated over a snow surface. The solar radiation is allowed to be absorbed only by the snow layer; thus, no solar penetration into the ice is considered.

There are three schemes for treating the sea ice albedo in the Noah sea ice module. One is a fixed value for the albedo; thus, seasonal variation and spatial distribution would not be taken into consideration. Another scheme uses the observed albedo through additional input data. The other scheme, which estimates the albedo as a function of surface temperature, is used in this study. Previous studies have shown that this empirical estimation of sea ice albedo could provide a result close to that obtained from observations in the Arctic during the summer melt season (Bromwich et al., 2009).

2.2 HIGHTSI

HIGHTSI was initially designed for seasonal ice simulation (Launiainen and Cheng, 1998; Vihma et al., 2002; Cheng et al., 2006), and it is also capable of being applied over perennial sea ice (Cheng et al., 2008b). Previous evaluations have shown that HIGHTSI can well simulate the seasonal evolution of Arctic sea ice temperature and thickness (Cheng et al., 2008b, 2013). Further studies have extended the use of HIGHTSI in investigating various processes. By combining the modeling with HIGHTSI and remote sensing data, an analysis that can better reveal the sea ice thickness and concentration information has been made (Karvonen et al., 2012). Moreover, HIGHTSI has also been used in lake ice studies (Yang et al., 2012), and its benefits from a detailed treatment of snow and ice thermodynamics have been confirmed when compared with a simple lake model (Semmler et al., 2012).

HIGHTSI contains multi-layer (up to 100) snow and ice such that the heat conduction in snow and ice can be represented in greater detail and the convergence of the nonlinear temperature solver can be better resolved (Dupont et al., 2015). The melt is calculated for each layer of snow and ice where the temperature would rise above the freezing point. After being reflected by the surface of sea ice and extincting in the snow layer, the solar radiation is then allowed to penetrate into the ice layers in HIGHTSI. During the ice melt season, the penetration of solar radiation into the ice layer

GMDD
8, 10305–10337, 2015

can warm the sea ice, thus causing ice ablation. The surface of sea ice in HIGHTSI is treated differently when it is covered by snow such that a more realistic seasonal feature of the sea ice surface can be represented in the model. Benefiting from the detailed representation of heat conduction and solar penetration in the sea ice, HIGHTSI is able to predict the change in sea ice thickness caused by thermodynamic processes. Note that dynamic processes play important roles in the change in sea ice thickness. A thermodynamic sea ice model cannot fully represent the ice thickness change if the sea ice dynamic processes there cannot be neglected.

The sea ice albedo scheme used in HIGTHSI is the same as the "CCSM" scheme used in the Community ICE Model (CICE) model (Collins et al., 2006). This scheme empirically estimates the albedo based on surface temperature, surface air temperature, snow cover and ice thickness.

Some modifications have been made to the snow processes in the original HIGHTSI model such that it can share some common physical assumptions with the snow over land and ice sheets in the WRF modeling system. The snow sublimation over sea ice is calculated using the same Penman equation used over land and ice sheets. The snow conduction as a function of snow density and the snow compaction effect as a function of temperature and time are also in accord with the empirical methods originally used by the Noah land surface module in WRF.

We added the HIGHTSI sea ice model as an option in the WRF modeling system such that it could be easily switched to use the Noah sea ice (hereafter WRF-Noah) or the HIGHTSI (hereafter WRF-HIGHTSI) sea ice through specifying a flag in the namelist file. When using the HIGHTSI option, the WRF model would provide precipitation, surface downward longwave and shortwave radiation, and air temperature, wind speed, and height of the lowest model level to drive the HIGHTSI model. HIGHTSI provides the updated surface temperature, albedo, emissivity, upward water vapor flux, and sensible and latent heat flux to WRF, which would then influence the atmospheric processes in the boundary layer.

GMDD
8, 10305–10337, 2015

2.3 Model setup

Two online simulations are performed: one using the original Polar WRF model and one using the Polar WRF model coupled with HIGHTSI. A domain in the western Arctic is used in this study (Fig. 2). This is the same as that used in the Arctic Regional Climate Model Intercomparison Project (Curry and Lynch, 2002, ARCMIP). Because the Surface Heat Budget of the Arctic Ocean (SHEBA) campaign was performed inside this domain, comprehensive in situ observations of high quality can be used to validate the simulation results. In this study, the horizontal resolution is set at 25 km, which was also used by Bromwich et al. (2009) in the same domain. Both perennial and first-year ice exist in this region, enabling us to evaluate the model's performance over different types of sea ice.

Because climate simulation is studied here, the model was freely integrated from 1 October 1997 to 1 November 1998 without any reinitialization during the simulation. This caused our results to differ from those in Bromwich et al. (2009), which reinitialized the model every 24 h from the ERA40 reanalysis. The initial and lateral boundary conditions are provided by ERA-Interim reanalysis, and the sea surface temperature (SST) and sea ice concentration are provided by the National Oceanic and Atmospheric Administration (NOAA) Optimal Interpolation SST analysis (OISST) version 2 and the National Aeronautics and Space Administration (NASA) bootstrap, respectively (Reynolds et al., 2002; Comiso and Nishio, 2008). The resolution of OISST is 0.25°, and that of NASA bootstrap is 25 km, which is close to the resolution of our simulation. The initial condition of snow depth on sea ice is provided by the Pan-Arctic-Ice-Ocean Modelling and Assimilation system (Zhang and Rothrock, 2003, PIOMAS), a reanalysis product with a resolution of approximately 25 km. Although HIGHTSI has the ability to simulate the change in sea ice thickness due to thermodynamic processes, the lack of a description of sea ice dynamics still made it difficult to well represent the thickness change over a large period. Consequently, the sea ice thickness in both PWRF and PWRF-HIGHTSI is updated by PIOMAS daily products. The sea ice thickness from

GMDD
8, 10305–10337, 2015

PIOMAS exhibits a similar pattern with observations (Laxon et al., 2013), and it has already been used as a boundary condition for simulations using the WRF model (Hines et al., 2015).

The simulation uses 38 eta vertical levels, among which at least 10 levels are within the planetary boundary layer. The top of the model is set at 10 hPa because a higher model top can reduce the bias in simulating the polar atmospheric circulation (Cassano et al., 2011). The time step for the simulation is 120 s. Spectral nudging at a wavelength of 1500 km is used because previous modeling studies have confirmed its benefit to the simulation over polar regions (Cassano et al., 2011).

The results in this study were based on version 3.6.1 of the Polar-modified WRF model, which was the latest release at the time of this study. For the choice of parameterization schemes, we used the same set as most of those used in the Arctic System Reanalysis (ASR) (Bromwich et al., 2015). Kain-Fritsch cumulus (Kain, 2004), Mellor-Yamada-Nakanishi-Niino (MYNN) 2.5-level planetary boundary layer (PBL) (Nakanish, 2001), Morrison two-moments microphysics (Morrison et al., 2009), and Noah land surface are used for the parameterization schemes in our simulation (Chen and Dudhia, 2001). For longwave and shortwave radiation, we use climate model-ready updates to the Rapid Radiative Transfer Model known as RRTMG (Iacono et al., 2008).

2.4 Data

The SHEBA experiment during 1997–1998 made comprehensive observations of the atmosphere, ocean and sea ice available (Uttal et al., 2002). The surface temperature, ice mass balance and ice temperature profiles are used to validate the sea ice simulation in this study. The atmospheric observations and the surface radiation observations are not only used in the model evaluations but also used as forcing data to drive the stand-alone versions of Noah sea ice and HIGHTSI. To validate the simulation over the entire model domain, satellite observations are also used. They are the skin surface temperature data from the Extended Advanced Very High Resolution Radiometer (AVHRR) Polar Pathfinder (APP-x) Product (Key et al., 1997) and the surface short-

GMDD
8, 10305–10337, 2015

wave and longwave radiation data from the European Organisation for the Exploitation of Meteorological Satellites (EUMETSAT) Climate Monitoring Satellite Application Facility (CM SAF) cLoud, Albedo and RAdiation dataset from AVHRR data (CLARA-A1) (Karlsson et al., 2013). Both APP-x and CLARA-A1 have similar spatial resolutions (25 km and 0.25°, respectively) as that used in our climate simulations. Validations with in situ observations have shown that both APP-x and CLARA-A1 have acceptable accuracies, and these products have already been used in model evaluations and climate change studies over the Arctic (Wang and Key, 2003; Svensson and Karlsson, 2011; Karlsson and Svensson, 2013; Koenigk et al., 2014; Riihelä et al., 2013).

3 Offline simulation of sea ice

The performance of HIGHTSI in simulating sea ice has been evaluated in previous studies, but a direct comparison between HIGHTSI and the sea ice module of Noah in WRF was not yet available (Cheng et al., 2008a). To determine the difference between HIGHTSI and Noah in simulating sea ice when given the observed atmospheric and oceanic forcing, the results from stand-alone versions of Noah sea ice and HIGHTSI are evaluated before they are coupled into the WRF modeling system. Following the settings of the Sea Ice Model Intercomparison Project Part 2 (SIMIP2) control experiment, atmospheric and radiation observations from SHEBA are used to drive the two offline sea ice models. The thickness and temperature of sea ice and the snow on sea ice are initiated with the results from the Pittsburgh site during the SHEBA field campaign (Perovich and Elder, 2001). The simulations start on 31 October 1997 and end on 22 September 1998 according to the temporal coverage of SHEBA data at the Pittsburgh site. The sea ice thickness is updated at every simulation step by the SHEBA observation for the Noah sea ice module because it is not able to predict the change in sea ice thickness. Benefiting from the more detailed description of thermodynamic processes of the sea ice in HIGHTSI, the sea ice thickness is predicted by the model itself for the HIGHTSI offline run. As mentioned above, snow is assumed to always

GMDD
8, 10305–10337, 2015

exist over the sea ice in Noah, and thus, a lower bound for snow depth needs to be specified. In this study, the minimum snow depth in Noah is set to 0.01 m, which is also the default value in the WRF modeling system.

The evolution of snow and sea ice temperature observed at Pittsburgh and simulated by Noah and HIGHTSI can be inferred from Fig. 1. Both Noah and HIGHTSI can well simulate the annual cycle of the sea ice temperature. A cold bias is observed in the simulation by Noah though most of the year, and the bias increases from the beginning of the simulation and becomes the largest in winter. It is colder than the SHEABA observation by more than 8° in the upper part of the sea ice in December and January. The snow depth simulated in Noah is considerably higher than the observation, which can lead to cold bias in the snow layer and upper part of sea ice. We performed a sensitivity experiment in which the snow depth in Noah is specified based on the SHEBA observation. The cold bias still exists in this simulation, implying that the overestimation of snow depth is not the only reason for the underestimation of sea ice temperature. Another experiment based on Noah is performed to determine to what extent the turbulent flux and albedo may contribute to the bias. In this simulation, the Noah sea ice model does not calculate turbulent fluxes and the surface temperature is specified based on the SHEBA observation. However, sea ice temperature is underestimated, and the bias in the upper part of the sea ice is over 6° during winter. Therefore, the bias in the sea ice simulation by Noah could result from the calculation of heat conduction inside the snow and ice. The sea ice temperature simulated by HIGHTSI, on the other hand, is warmer than the SHEABA observation during early spring. During other times of the year, the bias in the temperature simulation is rather small in HIGHTSI.

In general, the performance in simulating the sea ice temperature is better for HIGHTSI than for Noah, which can be inferred from the difference between the absolute biases of each model. As mentioned in Sect. 2, HIGHTSI has higher resolution and more sophisticated snow processes than Noah. Thus, the treatment of vertical heat conduction would be more complex in HIGHTSI than in Noah, which may lead to the better representation of sea ice temperature in HIGHTSI. Additionally, the temporal

GMDD
8, 10305–10337, 2015

evolution of sea ice thickness for HIGHTSI is calculated such that it is more consistent with the evolution of sea ice temperature. Because the purpose of this study is not to discuss the thermodynamic sea ice model in detail, a comprehensive evaluation of this offline simulation is not shown here. More of the evaluation on the HIGHTSI in simulating sea ice during SHEABA campaign can be seen in Cheng et al. (2008a).

4 Validation of the online simulation

The 6-hourly outputs from the simulation are bilinearly interpolated to the point where the SHEBA station was located at each time. Then, the monthly averages of the SHEBA observations and model results are compared (Fig. 3). WRF-Noah underestimates the surface temperature during winter compared with the SHEBA observation. The bias is approximately 5 to 6° from November to March, and it becomes smaller in summer when the sea ice temperature is close to its freezing point. WRF-HIGHTSI also underestimates the surface temperature in winter, but the bias is considerably smaller than that of WRF-Noah. The underestimation of both WRF-Noah and WRF-HIGHTSI is caused by an underestimation in downward longwave radiation. This is related to the misrepresentation of cloud microphysics, as revealed in previous evaluations (Wyser et al., 2007; Pithan et al., 2013). This bias in the cloud radiation effect in WRF-HIGHSI is partly compensated by its tendency for a warmer sea ice temperature. Considering the sea ice temperature (Fig. 4), cold biases remain in both WRF-Noah and WRF-HIGHTSI in the upper part of the sea ice during winter. The bias is larger in WRF-Noah than in WRF-HIGHTSI. ERA-Interim overestimates the sea ice surface temperature compared with the SHEBA observations. A recent study also found that the ERA-Interim simulates a warmer surface temperature over Antarctic ice sheet due to an overestimation of the surface turbulent fluxes under very stable conditions (Fréville et al., 2014; Jones and Lister, 2014). The surface air temperatures (at heights of 2.5 m for SHEBA observation and 2 m for ERA-Interim and WRF) simulated in WRF and ERA-Interim are also evaluated. Benefiting from the data assimilation, the results from ERA-Interim are the

GMDD
8, 10305–10337, 2015

closest with respect to the SHEBA observation. Both WRF-Noah and WRF-HIGHTSI underestimate the surface air temperature, whereas WRF-HIGHTSI has smaller bias than WRF-Noah.

Similar to the simulation of surface temperature, WRF-Noah underestimates the surface upward longwave radiation during winter. WRF-HIGHTSI, on the other hand, has better performance in simulating the upward longwave radiation than WRF-Noah due to the better representation of the surface temperature. Due to the smaller vertical gradient of sea ice temperature in summer, the bias becomes smaller for both the surface temperature and the upward longwave radiation. Moreover, the difference between WRF-HIGHTSI and WRF-Noah also becomes smaller in summer. Both WRF-Noah and WRF-HIGHTSI underestimate the surface upward shortwave radiation during late spring and early summer. This bias is caused by the underestimation of downward shortwave radiation. Both WRF-Noah and WRF-HIGHTSI overestimate the sea ice albedo due to the simulation of a too early snow melting over sea ice and the lack of melt-pond effect in summer. While the empirical estimate of sea ice albedo in WRF-Noah is better tuned for the summer sea ice in the Arctic (Bromwich et al., 2009), the higher upward shortwave radiation in WRF-HIGHTSI results from the overestimation of sea ice albedo.

In addition to the verification at the SHEBA site, the evaluation is also conducted over the entire domain covered by sea ice. Figure 5 shows the surface temperature, 2 m air temperature and surface upward longwave radiation from observations and their biases from WRF-Noah and WRF-HIGHTSI on January 1998. With reference to the satellite observation, the cold bias in simulating the surface temperature found at the SHEBA site can be observed anywhere that is covered by sea ice. The pattern of the bias in simulating the surface temperature was consistent with those in simulating the 2 m air temperature and surface upward longwave radiation. The biases were considerably smaller in WRF-HIGHTSI than in WRF-Noah over all the grid points covered by sea ice. A summary of the performance of WRF-HIGHTSI, WRF-Noah and ERA-Interim in simulating the surface temperature and radiation budget is given in terms of the metric

GMDD
8, 10305–10337, 2015

as root-mean-squared error (RMSE) with respect to observations (Fig. 6). In general, the RMSE was larger in winter than in summer, and WRF-HIGHTSI had a significantly smaller RMSE than WRF-Noah in winter.

5 Impact of the sea ice thickness specification

Previous studies have shown that sea ice thickness exerts a indiscernible influence on the atmosphere over sea ice (Gerdes, 2006; Krinner et al., 2009). It has been acknowledged that prescribing the sea ice fraction alone might lead to bias in the simulation of surface energy balance, particularly over the seasonal sea ice. To fulfill this demand, the ability to prescribe the observed sea ice thickness and the sea ice fraction is added to the recent versions of the WRF and Polar WRF models. Due to the difficulties in observing and retrieving the sea ice thickness, routinely reliable observations were not available at the time of this study. Some reanalysis products (such as PIOMAS used in this study) have provided useful information on the sea ice thickness with high spatial and temporal resolutions. However, note that the limited observations in the assimilation system can impact the quality of the sea ice reanalyses. Additionally, the surface energy imbalance could result from the inconsistency between the different sea ice in the reanalysis and that in the regional climate model. Currently, there are three ways to prescribe the sea ice thickness in the regional atmospheric model: treating sea ice as a constant value everywhere, using the spatially and temporally variant values from observations or reanalyses, or applying a simple parameterization based on the knowledge of the statistical relationship between sea ice thickness and sea ice fraction. The simple parameterization of sea ice thickness is represented in the form as the following equation, as first proposed by Krinner et al. (1997).

$$d = \left(0.2 + 3.8\left(f_{\min}^2\right)\right)\left(1 + 2\left(f - f_{\min}\right)\right) \quad (1)$$

GMDD
8, 10305–10337, 2015

The sea ice thickness estimated from this empirical method has proven to be close to the observational value in both Arctic and Antarctic sea ice in terms of the climatological mean.

Here, we present a new method for estimating the sea ice thickness, which incorporates both the empirical statistics as that in the simple parameterization and the potential ability of a complex thermodynamic sea ice model to predict the change in sea ice thickness. During the climate simulation of the regional climate model (WRF-HIGHTSI in this study), the sea ice thickness estimated from Eq. (1) is used as the initial value. Along with the integration of the RCM, the change in sea ice thickness is determined by the HIGHTSI component. For the grid point where no sea ice is present in the previous time step, the sea ice thickness is also prescribed from Eq. (1) as a first guess. In this way, the evolution of sea ice thickness is somewhat more reasonable than the value obtained only from the empirical method because the thermodynamic air–ice interaction could be resolved in RCM.

In addition to the two simulations evaluated in the previous section, three more simulations are performed to compare the simulations with different treatments of sea ice thickness. We use the same model as WRF-Noah in the previous section, but we fix the sea ice thickness as 3 m (hereafter referred to as Noah_3m), which is the default value in the WRF model when no additional information on sea ice thickness is given. The other two simulations use the WRF-HIGHTSI as was evaluated in the previous section. Among the two simulations, one is prescribed with the sea ice thickness estimated from the simple parameterization as given from Eq. (1) (hereafter referred to as PARAM), and the other one is prescribed with the sea ice thickness as proposed in terms of combining the empirical method and the prediction from HIGHTSI component (hereafter referred to as THERM). The sea ice thickness from the PIOMAS, the empirical estimation in PARAM and the results from THERM are presented in Fig. 7. Based on the results from PARAM, the perennial sea ice was approximately 3 m thick and the seasonal sea ice was less than 1 m thick. This empirical estimation could, to some extent, mimic the general climatology characteristics of the thickness distribution,

GMDD
8, 10305–10337, 2015

whereas it could not provide detailed information spatially and temporally. Based on the results from THERM, the sea ice thickness was similar with that from the PARAM when the model free run had just begun. Thus, it shared the same bias with that of PARAM. When the sea ice increased in thickness as predicted by the thermodynamic sea ice model, the bias became larger (smaller) over the perennial (seasonal) sea ice. Moreover, detailed spatial features of change in sea ice thickness could not be resolved in THERM because it could not account for the dynamic sea ice processes. Consequently, the THERM method could represent the seasonal evolution of sea ice thickness, but it would also depend on the initial guess that was estimated from the empirical parameterization. In our simulation, the THERM method showed better results than PARAM over seasonal sea ice, while it led to larger bias over perennial sea ice. The summary of the surface energy simulation over sea ice by prescribing different thermodynamic sea ice models and different treatments of sea ice thickness is given in Fig. 8. The RMSE was calculated from monthly mean values of surface temperature, surface upward longwave radiation, and 2 m air temperature simulated by the WRF model given different sea ice treatments through the simulation period from November 1997 to October 1998. Comparing the results from Noah and Noah_3m, prescribing observational information on the sea ice thickness led to a better simulation in the original polar-modified WRF. This result was consistent with Hines et al. (2015). Comparing the results from HIGHTSI, PARAM and THERM, it was found that the THERM method led to the largest error. Thus, we can conclude that it would be difficult for the thermodynamic sea ice model to well represent the sea ice thickness when there is a lack of consideration of dynamic processes and information on the initial guess.

6 Conclusions

As a major feature in the polar climate system, sea ice plays an important role in the air–ice–ocean interaction and needs to be properly represented in polar RCMs. The Noah sea ice model, which has been widely used in the WRF model, is compared with

GMDD
8, 10305–10337, 2015

a complex thermodynamic sea ice model, HIGHSI, in simulating the Arctic sea ice. Forced with atmospheric conditions observed during the SHEBA experiment, Noah sea ice exhibits cold bias during winter when simulating the sea ice temperature. Sensitivity experiments attributed this bias to not only the cloud radiation effect and stable boundary layer but also to heat conduction through snow and ice. HIGHTSI, which can better resolve the heat transport and solar penetration in snow and sea ice, provides a better simulation than Noah. To determine the possible added value from a complex thermodynamic sea ice model, HIGHTSI is coupled into the polar-modified WRF model. The evaluation of the model's simulation over sea ice surface is conducted using the SHEBA in situ observations and satellite radiation observations. The cold bias in simulating the surface temperature over sea ice in winter by WRF-Noah is reduced in the simulation of WRF-HIGHTSI, which also leads to a better representation of the surface upward longwave radiation and 2 m air temperature in the WRF-HIGHTSI.

The appropriate specification of sea ice thickness is important for climate simulations in the polar region. Regional climate simulations with sea ice thickness prescribed by different methods are conducted to study the impact from different treatments of sea ice thickness. Consistent with previous studies (Hines et al., 2015), prescribing the sea ice thickness with observational information results in the best simulation among all the other methods. If no observational information is available, using an empirical method based on the relationship between sea ice concentration and sea ice thickness could, to some extent, mimic the large-scale feature of the thickness distribution. In this study, we test another method in which the sea ice thickness is initialized from the empirical estimation and its change is predicted by the thermodynamic sea ice model itself. Based on this method, the large-scale feature of seasonal change in sea ice thickness can be better represented compared to the purely empirical estimation. However, its potential usage is still limited by the lack of dynamic sea ice processes and the coarse assumption on the initial sea ice thickness.

The simulation over sea ice surface is improved through coupling a complex thermodynamic sea ice model. Large bias in the surface radiation budget still exists due

GMDD
8, 10305–10337, 2015

to the misrepresentation of the cloud radiative effect. Thus, a better understanding of the cloud regime and developing a more sophisticated microphysics parameterization would greatly improve the model's simulation (Wesslén et al., 2014). In this study, only a thermodynamic sea ice model is coupled to the WRF because an interactive ocean model is not included here to drive the dynamic sea ice processes. The lack of sea ice dynamic processes means that the horizontal transport of mass and energy in sea ice is ignored in the regional atmospheric model, and thus, the model is still not sophisticated enough to well represent the air–ice–ocean interaction in the polar climate system. Therefore, although the development of coupled RCM is still a challenging task, it is an essential pathway toward a realistic simulation of the polar climate (Berg et al., 2015).

Code availability

The source code of WRF-HIGHTSI can be obtained at ftp://101.6.240.73/pub/WRF-HIGHTSI/WRF-HIGHTSI.tar.gz.

Acknowledgements. This study is supported by the National Basic Research Program of China (2013CBA01805).

References

Andreas, E. L., Persson, P. O. G., Grachev, A. A., Jordan, R. E., Horst, T. W., Guest, P. S., and Fairall, C. W.: Parameterizing turbulent exchange over sea ice in winter, J. Hydrometeorol., 11, 87–104, doi:10.1175/2009jhm1102.1, 2010. 10308

Barton, N. P., Klein, S. A., and Boyle, J. S.: On the contribution of longwave radiation to global climate model biases in arctic lower tropospheric stability, J. Climate, 27, 7250–7269, doi:10.1175/jcli-d-14-00126.1, 2014. 10307

Berg, P., Döscher, R., and Koenigk, T.: On the effects of constraining atmospheric circulation in a coupled atmosphere-ocean Arctic regional climate model, Clim. Dynam., doi:10.1007/s00382-015-2783-y, in press, 2015. 10323

GMDD
8, 10305–10337, 2015

Bitz, C. M. and Lipscomb, W. H.: An energy-conserving thermodynamic model of sea ice, J. Geophys. Res., 104, 15669, doi:10.1029/1999jc900100, 1999. 10308

Bourassa, M. A., Gille, S. T., Bitz, C., Carlson, D., Cerovecki, I., Clayson, C. A., Cronin, M. F., Drennan, W. M., Fairall, C. W., Hoffman, R. N., Magnusdottir, G., Pinker, R. T., Renfrew, I. A., Serreze, M., Speer, K., Talley, L. D., and Wick, G. A.: High-latitude ocean and sea ice surface fluxes: challenges for climate research, B. Am. Meteorol. Soc., 94, 403–423, doi:10.1175/bams-d-11-00244.1, 2013. 10307

Bromwich, D. H., Hines, K. M., and Bai, L.-S.: Development and testing of polar weather research and forecasting model: 2. Arctic Ocean, J. Geophys. Res.-Atmos., 114, D08122, doi:10.1029/2008JD010300, 2009. 10309, 10311, 10313, 10318

Bromwich, D. H., Otieno, F. O., Hines, K. M., Manning, K. W., and Shilo, E.: Comprehensive evaluation of polar weather research and forecasting model performance in the Antarctic, J. Geophys. Res.-Atmos., 118, 274–292, doi:10.1029/2012jd018139, 2013. 10309

Bromwich, D. H., Wilson, A. B., Bai, L.-S., Moore, G. W. K., and Bauer, P.: A comparison of the regional Arctic system reanalysis and the global ERA-interim reanalysis for the Arctic, Q. J. Roy. Meteor. Soc., doi:10.1002/qj.2527, in press, 2015. 10314

Cassano, J. J., Higgins, M. E., and Seefeldt, M. W.: Performance of the weather research and forecasting model for month-long Pan-Arctic simulations, Mon. Weather Rev., 139, 3469–3488, doi:10.1175/mwr-d-10-05065.1, 2011. 10308, 10314

Chen, F. and Dudhia, J.: Coupling an advanced land surface-hydrology model with the penn state-NCAR MM5 modeling system. Part I: Model implementation and sensitivity, Mon. Weather Rev., 129, 569–585, doi:10.1175/1520-0493(2001)129<0569:caalsh>2.0.CO;2, 2001. 10314

Cheng, B., Vihma, T., Pirazzini, R., and Granskog, M. A.: Modelling of superimposed ice formation during the spring snowmelt period in the Baltic Sea, Ann. Glaciol., 44, 139–146, doi:10.3189/172756406781811277, 2006. 10311

Cheng, B., Vihma, T., Zhang, Z.-h., Zhi-jun, L., and Hui-ding, W.: Snow and sea ice thermodynamics in the Arctic: Model validation and sensitivity study against SHEBA data, Chinese Journal of Polar Science, 19, 108–122, doi:CNKI:SUN:JDYJ.0.2008-02-003, 2008a. 10315, 10317

Cheng, B., Zhang, Z., Vihma, T., Johansson, M., Bian, L., Li, Z., and Wu, H.: Model experiments on snow and ice thermodynamics in the Arctic Ocean with CHINARE 2003 data, J. Geophys. Res.-Oceans, 113, C09020, doi:10.1029/2007JC004654, 2008b. 10311

GMDD
8, 10305–10337, 2015

Cheng, B., Mäkynen, M., Similä, M., Rontu, L., and Vihma, T.: Modelling snow and ice thickness in the coastal Kara Sea, Russian Arctic, Ann. Glaciol., 54, 105–113, doi:10.3189/2013aog62a180, 2013. 10311
Collins, W. D., Bitz, C. M., Blackmon, M. L., Bonan, G. B., Bretherton, C. S., Carton, J. A., Chang, P., Doney, S. C., Hack, J. J., Henderson, T. B., Kiehl, J. T., Large, W. G., McKenna, D. S., Santer, B. D., and Smith, R. D.: The community climate system model version 3 (CCSM3), J. Climate, 19, 2122–2143, doi:10.1175/jcli3761.1, 2006. 10312
Comiso, J. C. and Nishio, F.: Trends in the sea ice cover using enhanced and compatible AMSR-E, SSM/I, and SMMR data, J. Geophys. Res., 113, C02S07, doi:10.1029/2007jc004257, 2008. 10313
Curry, J. A. and Lynch, A. H.: Comparing arctic regional climate model, EOS T. Am. Geophys. Un., 83, p. 87, doi:10.1029/2002EO000051, 2002. 10313
Dorn, W., Dethloff, K., and Rinke, A.: Improved simulation of feedbacks between atmosphere and sea ice over the Arctic Ocean in a coupled regional climate model, Ocean Model., 29, 103–114, doi:10.1016/j.ocemod.2009.03.010, 2009. 10308
Dorn, W., Dethloff, K., and Rinke, A.: Limitations of a coupled regional climate model in the reproduction of the observed Arctic sea-ice retreat, The Cryosphere, 6, 985–998, doi:10.5194/tc-6-985-2012, 2012. 10308
Dupont, F., Vancoppenolle, M., Tremblay, L.-B., and Huwald, H.: Comparison of different numerical approaches to the 1D sea-ice thermodynamics problem, Ocean Model., 87, 20–29, doi:10.1016/j.ocemod.2014.12.006, 2015. 10311
English, J. M., Gettelman, A., and Henderson, G. R.: Arctic radiative fluxes: present-day biases and future projections in CMIP5 models, J. Climate, 28, 6019–6038, doi:10.1175/jcli-d-14-00801.1, 2015. 10307
Fréville, H., Brun, E., Picard, G., Tatarinova, N., Arnaud, L., Lanconelli, C., Reijmer, C., and van den Broeke, M.: Using MODIS land surface temperatures and the Crocus snow model to understand the warm bias of ERA-Interim reanalyses at the surface in Antarctica, The Cryosphere, 8, 1361–1373, doi:10.5194/tc-8-1361-2014, 2014. 10317
Gerdes, R.: Atmospheric response to changes in Arctic sea ice thickness, Geophys. Res. Lett., 33, L18709, doi:10.1029/2006gl027146, 2006. 10319
Glisan, J. M. and Gutowski, W. J.: WRF summer extreme daily precipitation over the CORDEX Arctic, J. Geophys. Res.-Atmos., 119, 1720–1732, doi:10.1002/2013jd020697, 2014a. 10309

GMDD
8, 10305–10337, 2015

Glisan, J. M. and Gutowski, W. J.: WRF winter extreme daily precipitation over the North American CORDEX Arctic, J. Geophys. Res.-Atmos., 119, 10738–10748, doi:10.1002/2014JD021676, 2014JD021676, 2014b. 10309

Hines, K. M. and Bromwich, D. H.: Development and testing of polar weather research and forecasting (WRF) model. Part I: Greenland ice sheet meteorology, Mon. Weather Rev., 136, 1971–1989, doi:10.1175/2007mwr2112.1, 2008. 10309, 10310

Hines, K. M., Bromwich, D. H., Bai, L.-S., Barlage, M., and Slater, A. G.: Development and testing of polar WRF. Part III: Arctic land, J. Climate, 24, 26–48, doi:10.1175/2010jcli3460.1, 2011. 10309

Hines, K. M., Bromwich, D. H., Bai, L., Bitz, C. M., Powers, J. G., and Manning, K. W.: Sea ice enhancements to polar WRF, Mon. Weather Rev., 143, 2363–2385, 2015. 10308, 10310, 10314, 10321, 10322

Iacono, M. J., Delamere, J. S., Mlawer, E. J., Shephard, M. W., Clough, S. A., and Collins, W. D.: Radiative forcing by long-lived greenhouse gases: calculations with the AER radiative transfer models, J. Geophys. Res., 113, D13103, doi:10.1029/2008jd009944, 2008. 10314

Jin, Z., Stamnes, K., Weeks, W. F., and Tsay, S.-C.: The effect of sea ice on the solar energy budget in the atmosphere-sea ice-ocean system: A model study, J. Geophys. Res.-Oceans, 99, 25281–25294, doi:10.1029/94JC02426, 1994. 10308

Jones, P. D. and Lister, D. H.: Antarctic near-surface air temperatures compared with ERA-Interim values since 1979, Int. J. Climatol., 35, 1354–1366, doi:10.1002/joc.4061, 2014. 10317

Kain, J. S.: The Kain–Fritsch convective parameterization: an update, J. Appl. Meteorol., 43, 170–181, doi:10.1175/1520-0450(2004)043<0170:tkcpau>2.0.co;2, 2004. 10314

Karlsson, J. and Svensson, G.: Consequences of poor representation of Arctic sea-ice albedo and cloud-radiation interactions in the CMIP5 model ensemble, Geophys. Res. Lett., 40, 4374–4379, doi:10.1002/grl.50768, 2013. 10315

Karlsson, K.-G., Riihelä, A., Müller, R., Meirink, J. F., Sedlar, J., Stengel, M., Lockhoff, M., Trentmann, J., Kaspar, F., Hollmann, R., and Wolters, E.: CLARA-A1: a cloud, albedo, and radiation dataset from 28 yr of global AVHRR data, Atmos. Chem. Phys., 13, 5351–5367, doi:10.5194/acp-13-5351-2013, 2013. 10315

Karvonen, J., Cheng, B., Vihma, T., Arkett, M., and Carrieres, T.: A method for sea ice thickness and concentration analysis based on SAR data and a thermodynamic model, The Cryosphere, 6, 1507–1526, doi:10.5194/tc-6-1507-2012, 2012. 10311

GMDD
8, 10305–10337, 2015

Key, J. R., Collins, J. B., Fowler, C., and Stone, R. S.: High-latitude surface temperature estimates from thermal satellite data, Remote Sens. Environ., 61, 302–309, doi:10.1016/S0034-4257(97)89497-7, 1997. 10314
Koenigk, T., Devasthale, A., and Karlsson, K.-G.: Summer Arctic sea ice albedo in CMIP5 models, Atmos. Chem. Phys., 14, 1987–1998, doi:10.5194/acp-14-1987-2014, 2014. 10315
Koenigk, T., Berg, P., and D?scher, R.: Arctic climate change in an ensemble of regional CORDEX simulations, Polar Res., 34, 24603, doi:10.3402/polar.v34.24603, 2015. 10307
Krinner, G., Genthon, C., Li, Z.-X., and Le Van, P.: Studies of the Antarctic climate with a stretched-grid general circulation model, J. Geophys. Res.-Atmos., 102, 13731–13745, doi:10.1029/96JD03356, 1997. 10319
Krinner, G., Rinke, A., Dethloff, K., and Gorodetskaya, I. V.: Impact of prescribed Arctic sea ice thickness in simulations of the present and future climate, Clim. Dynam., 35, 619–633, doi:10.1007/s00382-009-0587-7, 2009. 10319
Launiainen, J. and Cheng, B.: Modelling of ice thermodynamics in natural water bodies, Cold Reg. Sci. Technol., 27, 153–178, 1998. 10311
Laxon, S. W., Giles, K. A., Ridout, A. L., Wingham, D. J., Willatt, R., Cullen, R., Kwok, R., Schweiger, A., Zhang, J., Haas, C., Hendricks, S., Krishfield, R., Kurtz, N., Farrell, S., and Davidson, M.: CryoSat-2 estimates of Arctic sea ice thickness and volume, Geophys. Res. Lett., 40, 732–737, doi:10.1002/grl.50193, 2013. 10314
Liu, F., Krieger, J. R., and Zhang, J.: Toward producing the Chukchi–Beaufort High-Resolution Atmospheric Reanalysis (CBHAR) via the WRFDA data assimilation system, Mon. Weather Rev., 142, 788–805, 2014. 10310
Morrison, H., Thompson, G., and Tatarskii, V.: Impact of cloud microphysics on the development of trailing stratiform precipitation in a simulated squall line: comparison of one- and two-moment schemes, Mon. Weather Rev., 137, 991–1007, doi:10.1175/2008mwr2556.1, 2009. 10314
Nakanish, M.: Improvement of the Mellor–Yamada turbulence closure model based on large-eddy simulation data, Bound.-Lay. Meteorol., 99, 349–378, doi:10.1023/a:1018915827400, 2001. 10314
Notz, D.: Challenges in simulating sea ice in Earth System Models, WIREs Clim Change, 3, 509–526, doi:10.1002/wcc.189, 2012. 10307
Perovich, D. K. and Elder, B. C.: Temporal evolution of Arctic sea-ice temperature, Ann. Glaciol., 33, 207–211, doi:10.3189/172756401781818158, 2001. 10315

GMDD
8, 10305–10337, 2015

Pithan, F., Medeiros, B., and Mauritsen, T.: Mixed-phase clouds cause climate model biases in Arctic wintertime temperature inversions, Clim. Dynam., 43, 289–303, doi:10.1007/s00382-013-1964-9, 2013. 10307, 10317

Reynolds, R. W., Rayner, N. A., Smith, T. M., Stokes, D. C., and Wang, W.: An improved in situ and satellite SST analysis for climate, J. Climate, 15, 1609–1625, doi:10.1175/1520-0442(2002)015<1609:aiisas>2.0.co;2, 2002. 10313

Riihelä, A., Manninen, T., and Laine, V.: Observed changes in the albedo of the Arctic sea-ice zone for the period 1982–2009, Nature Climate Change, 3, 895–898, doi:10.1038/nclimate1963, 2013. 10315

Rinke, A., Maslowski, W., Dethloff, K., and Clement, J.: Influence of sea ice on the atmosphere: a study with an Arctic atmospheric regional climate model, J. Geophys. Res., 111, D16103, doi:10.1029/2005jd006957, 2006. 10308

Semmler, T., Cheng, B., Yang, Y., and Rontu, L.: Snow and ice on Bear Lake (Alaska) a sensitivity experiments with two lake ice models, Tellus A, 64, 17339, doi:10.3402/tellusa.v64i0.17339, 2012. 10311

Sorteberg, A., Kattsov, V., Walsh, J. E., and Pavlova, T.: The Arctic surface energy budget as simulated with the IPCC AR4 AOGCMs, Clim. Dynam., 29, 131–156, doi:10.1007/s00382-006-0222-9, 2007. 10307

Steeneveld, G. J., van de Wiel, B. J. H., and Holtslag, A. A. M.: Modeling the evolution of the atmospheric boundary layer coupled to the land surface for three contrasting nights in CASES-99, J. Atmos. Sci., 63, 920–935, doi:10.1175/jas3654.1, 2006. 10307

Sterk, H. A. M., Steeneveld, G. J., and Holtslag, A. A. M.: The role of snow-surface coupling, radiation, and turbulent mixing in modeling a stable boundary layer over Arctic sea ice, J. Geophys. Res.-Atmos., 118, 1199–1217, doi:10.1002/jgrd.50158, 2013. 10307

Svensson, G. and Karlsson, J.: On the Arctic wintertime climate in global climate models, J. Climate, 24, 5757–5771, doi:10.1175/2011jcli4012.1, 2011. 10315

Tjernström, M., Sedlar, J., and Shupe, M. D.: How well do regional climate models reproduce radiation and clouds in the Arctic? An evaluation of ARCMIP simulations, J. Appl. Meteorol. Clim., 47, 2405–2422, doi:10.1175/2008jamc1845.1, 2008. 10307

Uttal, T., Curry, J. A., Mcphee, M. G., Perovich, D. K., Moritz, R. E., Maslanik, J. A., Guest, P. S., Stern, H. L., Moore, J. A., Turenne, R., Heiberg, A., Serreze, M. C., Wylie, D. P., Persson, O. G., Paulson, C. A., Halle, C., Morison, J. H., Wheeler, P. A., Makshtas, A., Welch, H., Shupe, M. D., Intrieri, J. M., Stamnes, K., Lindsey, R. W., Pinkel, R., Pegau, W. S., Stan-

GMDD
8, 10305–10337, 2015

ton, T. P., and Grenfeld, T. C.: Surface heat budget of the Arctic ocean, B. Am. Meteorol. Soc., 83, 255–275, doi:10.1175/1520-0477(2002)083<0255:shbota>2.3.co;2, 2002. 10314
Vihma, T. and Pirazzini, R.: On the factors controlling the snow surface and 2-m air temperatures over the Arctic sea ice in winter, Bound.-Lay. Meteorol., 117, 73–90, doi:10.1007/s10546-004-5938-7, 2005. 10307
Vihma, T., Uotila, J., Cheng, B., and Launiainen, J.: Surface heat budget over the Weddell Sea: buoy results and model comparisons, J. Geophys. Res.-Oceans, 107, 5-1–5-15, doi:10.1029/2000JC000372, 2002. 10311
Wang, X. and Key, J. R.: Recent trends in Arctic surface, cloud, and radiation properties from space, Science, 299, 1725–1728, doi:10.1126/science.1078065, 2003. 10315
Wang, Y. and Liu, X.: Immersion freezing by natural dust based on a soccer ball model with the Community Atmospheric Model version 5: climate effects, Environ. Res. Lett., 9, 124020, doi:10.1088/1748-9326/9/12/124020, 2014. 10308
Wesslén, C., Tjernström, M., Bromwich, D. H., de Boer, G., Ekman, A. M. L., Bai, L.-S., and Wang, S.-H.: The Arctic summer atmosphere: an evaluation of reanalyses using ASCOS data, Atmos. Chem. Phys., 14, 2605–2624, doi:10.5194/acp-14-2605-2014, 2014. 10323
Wyser, K., Jones, C. G., Du, P., Girard, E., Willén, U., Cassano, J., Christensen, J. H., Curry, J. A., Dethloff, K., Haugen, J.-E., Jacob, D., Køltzow, M., Laprise, R., Lynch, A., Pfeifer, S., Rinke, A., Serreze, M., Shaw, M. J., Tjernström, M., and Zagar, M.: An evaluation of Arctic cloud and radiation processes during the SHEBA year: simulation results from eight Arctic regional climate models, Clim. Dynam., 30, 203–223, doi:10.1007/s00382-007-0286-1, 2007. 10307, 10317
Yang, Y., Leppäranta, M., Cheng, B., and Li, Z.: Numerical modelling of snow and ice thicknesses in Lake Vanajavesi, Finland, Tellus A, 64, 17202, doi:10.3402/tellusa.v64i0.17202, 2012. 10311
Zhang, J. and Rothrock, D. A.: Modeling global sea ice with a thickness and enthalpy distribution model in generalized curvilinear coordinates, Mon. Weather Rev., 131, 845–861, doi:10.1175/1520-0493(2003)131<0845:mgsiwa>2.0.co;2, 2003. 10313

GMDD
8, 10305–10337, 2015

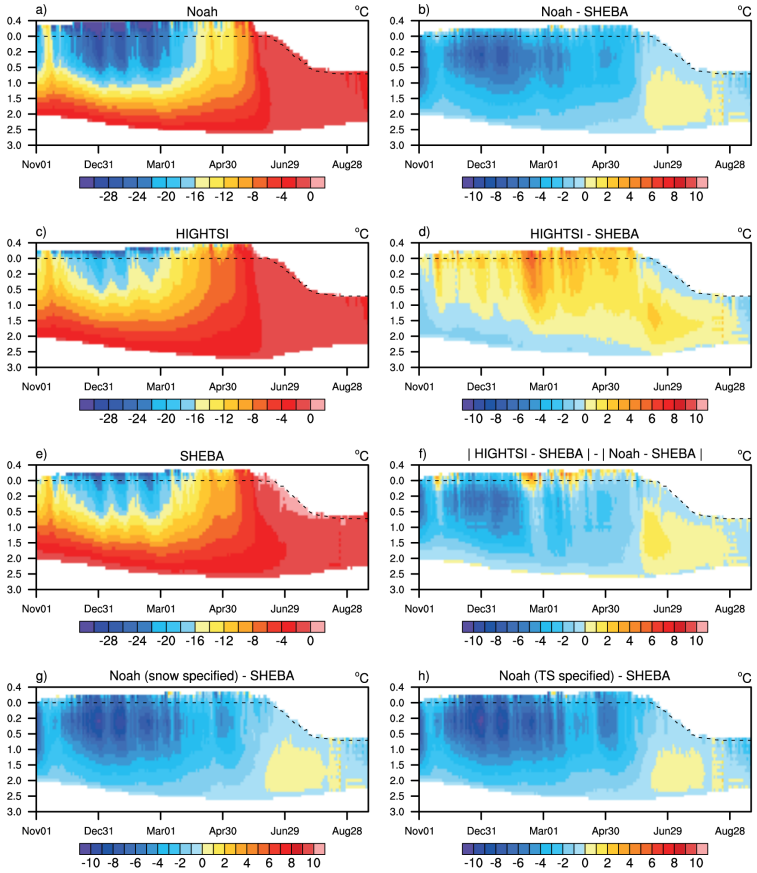

Figure 1. The evolution of sea ice temperature: results from **(a)** Noah, **(c)** HIGHTSI and **(e)** SHEBA observation; bias of **(b)** Noah, **(d)** HIGHTSI, **(g)** Noah with specified snow depth on sea ice, and **(h)** Noah with specified snow depth and surface temperature on sea ice; and **(f)** the difference between the absolute bias of HIGHTSI and SHEBA.

GMDD
8, 10305–10337, 2015

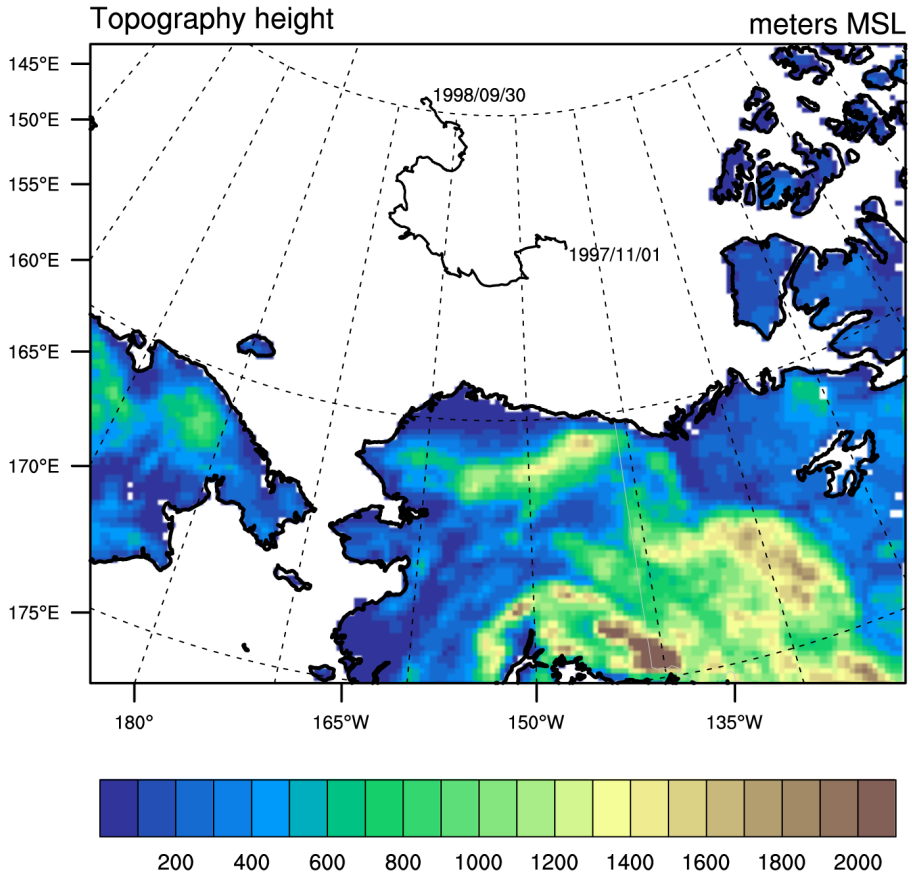

Figure 2. Topography of the simulation domain. SHEBA site locations are marked by the black curve.

GMDD
8, 10305–10337, 2015

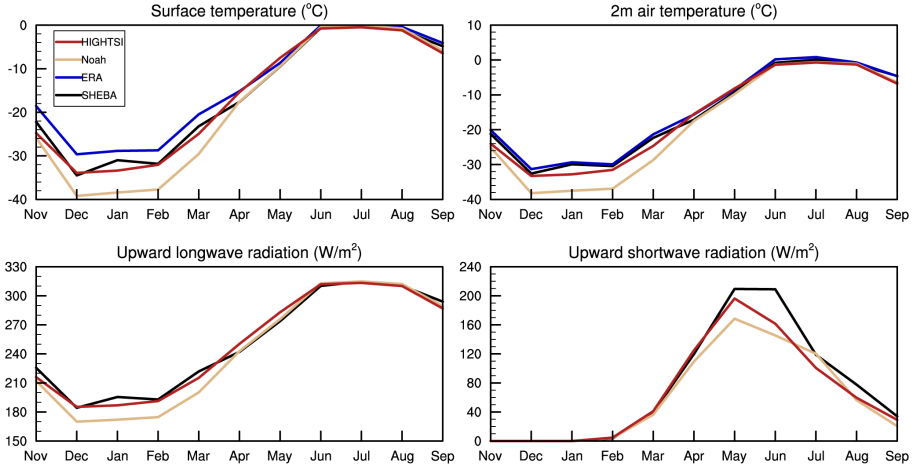

Figure 3. Monthly mean surface temperature, 2 m air temperature and surface upward longwave and shortwave radiation simulated and observed at the SHEBA sites.

GMDD
8, 10305–10337, 2015

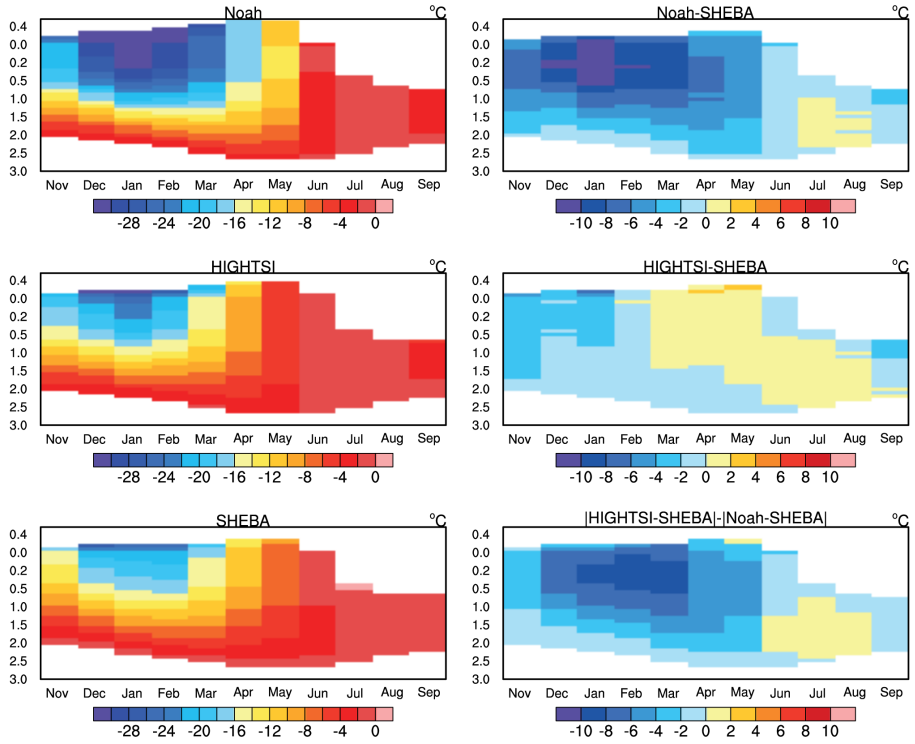

Figure 4. The evolution of monthly mean sea ice temperature: (left) results from (top) Noah, (mid) HIGHTSI and (bottom) SHEBA observation; (right) bias of (top) Noah and (mid) HIGHTSI; and (bottom right) the difference between the absolute bias of HIGHTSI and SHEBA.

GMDD
8, 10305–10337, 2015

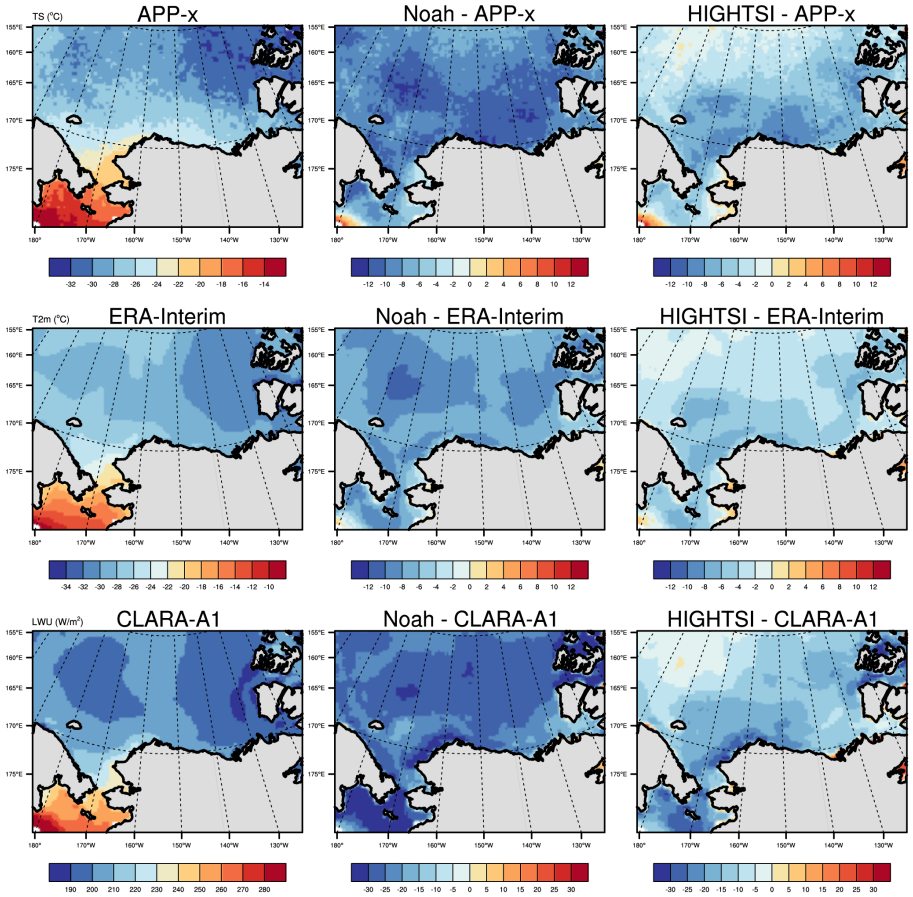

Figure 5. Surface temperature, 2 m air temperature and surface upward longwave radiation over sea ice surface in January 1998: (left) observations and bias in (mid) Noah and (right) HIGHTSI.

GMDD
8, 10305–10337, 2015

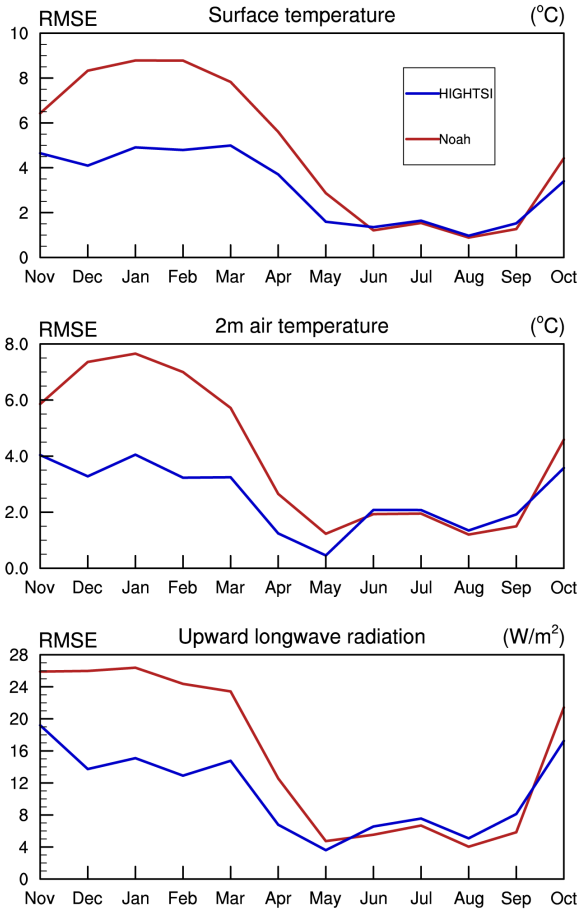

Figure 6. RMSE of surface temperature, 2 m air temperature and upward longwave radiation for WRF-Noah and WRF-HIGHTSI.

GMDD
8, 10305–10337, 2015

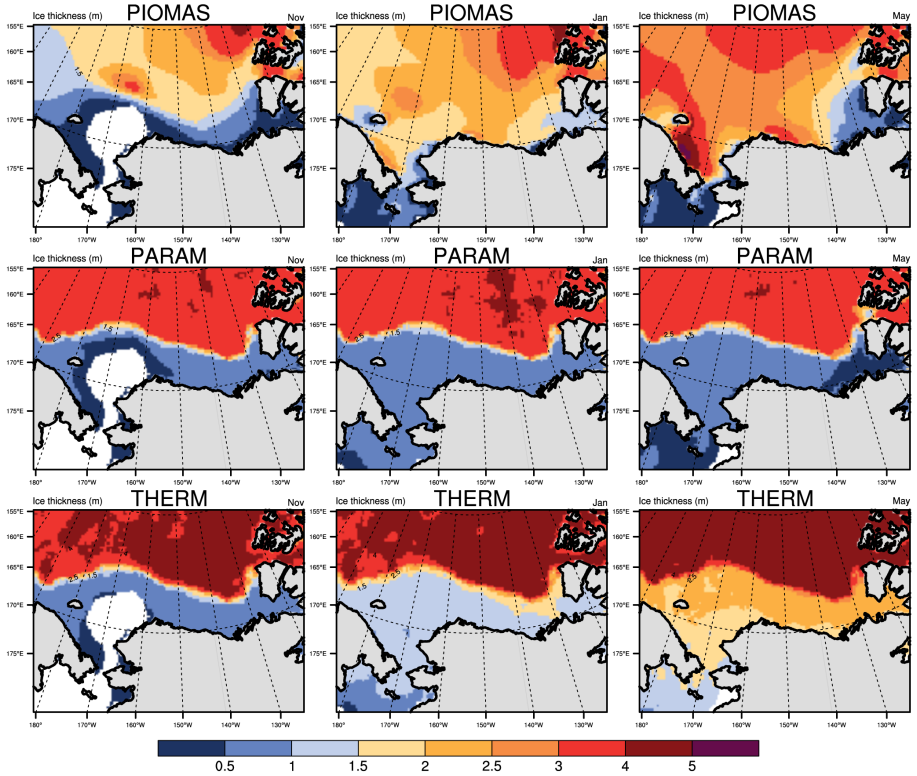

Figure 7. Sea ice thickness in (left) PIOMAS, (mid) PARAM and (bottom) THERM during (left) November 1997, (mid) January 1998 and (right) May 1998.

GMDD
8, 10305–10337, 2015

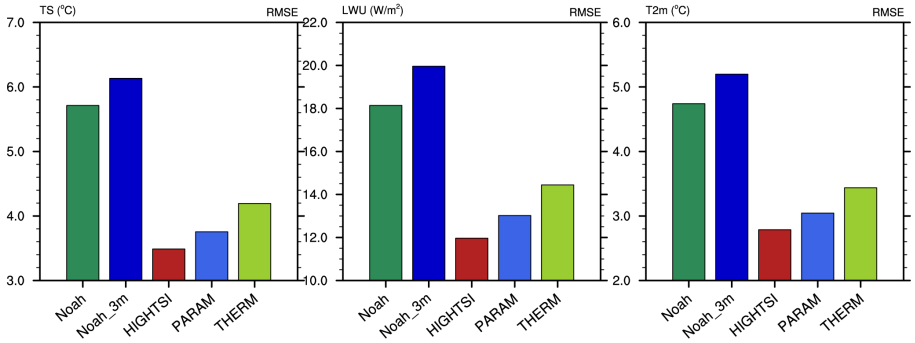

Figure 8. RMSE of surface temperature, upward longwave radiation and 2 m air temperature for WRF-Noah and WRF-HIGHTSI prescribed with different sea ice thicknesses.

GMDD
8, 10305–10337, 2015